On the use of flexural wave propagation experiments for identification of complex modulus *

Kaushik Mahata†, Torsten Söderström†, Magnus Mossberg†,
Lars Hillström‡ and Saed Mousavi‡

† Department of Systems and Control, Information Technology,
Uppsala University, P O Box 27, SE-751 03 Uppsala, Sweden

‡ Solid Mechanics, Department of Material Science, Ångström Laboratory
Uppsala University, P O Box 534, SE-751 21 Uppsala, Sweden

version November 14, 2001

Abstract

In this paper, we investigate the estimation of the complex modulus of a viscoelastic material from flexural wave experiments. A bar specimen of uniform cross-section is subjected to lateral impact by a steel ball giving rise to flexural waves traveling along the bar. The strains due to wave propagation are registered as functions of time using strain gauges at different sections. The measured strains are transformed into the frequency domain. A non-parametric estimation of the complex modulus is carried out for each frequency. An analysis of the quality of the non-parametric estimate is carried out. The validity of the theoretical results are confirmed by numerical studies and experimental tests.

*This work was supported by Swedish Research Council for Engineering Sciences under contract 2000-587.

1 Introduction

The frequency dependent complex modulus relates the stress and the strain in a viscoelastic material when it is subjected to dynamic load variation [4]. The resulting waves of different frequencies have different wavelengths, speeds and attenuation rates. Polymers are examples of viscoelastic materials. In order to make efficient use of a viscoelastic material, it is important to know its complex modulus at different frequencies. When the components and structures are loaded dynamically, the frequencies of interest may vary between 10 Hz and 1 kHz. In this range wave propagation methods [1] are well suited for the determination of the complex modulus. An experiment as in Figure 1 is carried out. A bar specimen is

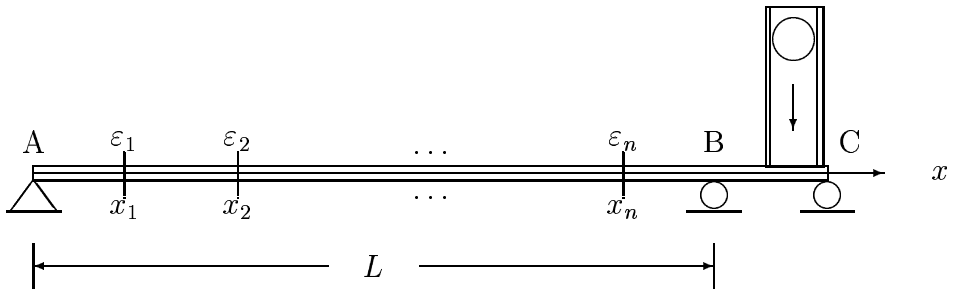

Figure 1: Experimental set up.

impacted laterally by a steel ball giving rise to flexural waves traveling along the bar. The strains due to the wave propagation are registered using strain gauges at sections $\{x_i\}_{i=1}^n$. The analog strain data are passed through an anti-aliasing filter and discretised. The discretised data are subjected to Discrete Fourier Transform (DFT) to get a frequency-domain description [12]. A non-parametric identification of the complex modulus is carried out for each frequency. Similar approaches for evaluating material parameters can also be found in [7], [8], [10].

It is important to know the accuracy of the estimated complex modulus. This type of accuracy analysis can be used to design an optimal experiment, for example to find out the sensor configuration, so that the estimates have the least possible variance. It turns out that it is difficult to get an accurate estimate at certain frequencies if all the sensors are equidistant [8]. An analysis of the accuracy of the complex modulus estimate using extensional wave experiments is given in [11]. In this paper we briefly outline the flexural wave propagation in a homogeneous viscoelastic bar of uniform cross-section. The differential equations governing the strains are solved for each frequency. The structure of the solution is then exploited to set up a separable non-linear least squares problem, to be solved in order to estimate the complex elastic modulus. An analysis of the quality of the non-parametric estimate is carried out. In the analysis, the measurements are assumed to be corrupted by additive white noise. Using the analytical results, we shall give further insight into the nature of the estimates obtained and discuss their dependence on experimental parameters. We shall show that for a high signal to noise ratio of the measured strain data, the real and the imaginary parts of the complex modulus estimate at a given frequency have equal variances and

are statistically uncorrelated. Moreover, the variance at a particular frequency is inversely proportional to the signal to noise ratio at that frequency. The validity of the analytical results will be confirmed by numerical studies and real experiments. We also address some numerical issues involved in the algorithm and present some ways to handle them.

The paper is structured as follows. In the next section, we present briefly the dynamics of flexural wave propagation in a bar specimen. The non-parametric identification method and its accuracy are discussed in Section 3. In Section 4, the theoretical results are illustrated using a numerical simulation study. In Section 5, we describe the results from the experiments and validate the theoretical results in a real scenario.

2 System description

Consider the segment AB of the homogeneous Timoshenko beam [7] in Figure 1, which is of uniform cross-sectional area A and moment of inertia I. Let x be the co-ordinate along the straight centre-line of the beam. Let the material be *linearly viscoelastic* with density ρ and frequency dependent complex modulus $\mathcal{E}(\omega)$, where we denote the angular frequency in rad/sec by ω. It is assumed that within the beam segment of length L under consideration, there are no external load, support, joint or spot of contact with any other body. The beam segment is at rest for time $t < 0$, while it is traversed by flexural waves for $t \geq 0$ due to a load of finite duration outside the segment under study. The bending moment $M(x,t)$ and the shear force $Q(x,t)$ at any section x at time t are related to the rotational velocity $\dot{\phi}(x,t)$ and $\dot{w}(x,t)$, the time derivative of the centre-line deflection, see [7] for details. These quantities constitute the state vector

$$\mathbf{s}(x,t) = \left[\begin{array}{cccc} Q(x,t) & \dot{w}(x,t) & M(x,t) & \dot{\phi}(x,t) \end{array} \right]^{\mathrm{T}}. \tag{2.1}$$

In frequency domain, the state vector follows a system of first order ordinary differential equations [7] given by

$$\frac{d\mathbf{S}(x,\omega)}{dx} = \mathbf{R}(\omega)\mathbf{S}(x,\omega), \tag{2.2}$$

where we denote the Fourier transform of the vector $\mathbf{s}(x,t)$ by $\mathbf{S}(x,\omega)$ and

$$\mathbf{R}(\omega) = \left[\begin{array}{cccc} 0 & \mathrm{i}\omega\rho A & 0 & 0 \\ \frac{\mathrm{i}\omega\psi}{A\mathcal{E}(\omega)} & 0 & 0 & -1 \\ 1 & 0 & 0 & \mathrm{i}\omega\rho I \\ 0 & 0 & \frac{\mathrm{i}\omega}{I\mathcal{E}(\omega)} & 0 \end{array} \right]. \tag{2.3}$$

Note that, we have introduced a known constant ψ, which depends upon the cross-sectional geometry and the complex Poission's ratio of the material. The Poission's ratio is assumed to be known. The general solution to (2.2) is given by

$$\mathbf{S}(x,\omega) = \mathbf{c}_1(\omega)\mathrm{e}^{\gamma_1(\omega)x} + \mathbf{c}_2(\omega)\mathrm{e}^{\gamma_2(\omega)x} + \mathbf{c}_3(\omega)\mathrm{e}^{-\gamma_1(\omega)x} + \mathbf{c}_4(\omega)\mathrm{e}^{-\gamma_2(\omega)x}, \tag{2.4}$$

where $\{\pm\gamma_i(\omega)\}_{i=1}^2$ are the eigenvalues of $\mathbf{R}(\omega)$. They are commonly referred as the wave propagation functions. The vectors $\{\mathbf{c}_i(\omega)\}_{i=1}^4$ depend upon the boundary conditions. In order to solve for the eigenvalues of $\mathbf{R}(\omega)$, we need to solve the characteristic equation of $\mathbf{R}(\omega)$, which is given by

$$\gamma^4 + 2a(\omega)\gamma^2 - b(\omega) = 0, \tag{2.5}$$

where

$$a(\omega) = \frac{\rho\omega^2}{2\mathcal{E}(\omega)}\left[1+\psi\right], \tag{2.6}$$

$$b(\omega) = \frac{\rho\omega^2}{\mathcal{E}(\omega)}\left[\frac{A}{I} - \frac{\rho\omega^2}{\mathcal{E}(\omega)}\psi\right]. \tag{2.7}$$

Hence from (2.5), the wave propagation functions are given by

$$\gamma_1^2(\omega) = -a(\omega) + \sqrt{a^2(\omega)+b(\omega)}, \tag{2.8}$$

$$\gamma_2^2(\omega) = -a(\omega) - \sqrt{a^2(\omega)+b(\omega)}. \tag{2.9}$$

We note in passing that each component of the state vector $\mathbf{S}(x,\omega)$ is composed of the contributions of two different waves corresponding to the propagation constants $\gamma_1(\omega)$ and $\gamma_2(\omega)$ respectively. Moreover, $\gamma_i(\omega)$ corresponds to the wave propagation in the negetive x direction, and $-\gamma_i(\omega)$ represents the reflected wave in the positive x direction, see Figure 1. The vectors $\{\mathbf{c}_i(\omega)\}_{i=1}^4$ are the amplitudes of the associated waves at $x = 0$.

3 Identification of the complex modulus

In this section, we consider the identification of the complex modulus $\mathcal{E}(\omega)$ from the sampled strain data in a set of predefined sections $\{x_i\}_{i=1}^n$ on the beam, as shown in Figure 1, measured at time instants $\{kT\}_{k=0}^{N-1}$, where T denotes the sampling interval. For notational simplicity, we refer to any signal $X(kT)$ by $X(k)$. The measured strains are transformed to the frequency domain using the Discrete Fourier transform (DFT) to obtain strains at N discrete frequencies given by

$$\omega_k = \begin{cases} \frac{2\pi k}{NT}, & 0 \le k \le \frac{N}{2} \\ \frac{2\pi(k-N)}{NT}, & \frac{N}{2} < k < N \end{cases}. \tag{3.1}$$

Since the measured signals are real-valued, it is sufficient to consider only the positive frequencies. Thus we shall consider only

$$\omega_k = \frac{2\pi k}{NT}, \quad 0 < k < \tfrac{N}{2} \tag{3.2}$$

in our analysis. The maximum frequency that can be observed is $\frac{1}{2T}$ Hz. In order to avoid aliasing, it is necessary to filter the strain signals by an anti-aliasing filter before sampling. The anti-aliasing filter should be of low-pass characteristic and with the cut-off frequency f_c at most at $\frac{1}{2T}$ Hz. Let the maximum frequency at

which we need to estimate $\mathcal{E}(\omega)$ be $f_{\max}$ and the transition band of the anti-aliasing filter be B. Then we must have

$$f_{\max} \leq f_c - B \leq \frac{1}{2T} - B \quad \Rightarrow T \leq \frac{1}{2\,(f_{\max} + B)}. \tag{3.3}$$

The resolution in the frequency domain is $\frac{1}{NT}$. Thus, a required resolution in the frequency domain sets a lower bound on N.

The true strain $\varepsilon(x, \omega)$ at a section x and frequency ω is directly proportional to the bending moment at that section and at that frequency. The constant of proportionality is $\frac{A}{I\mathcal{E}(\omega)}$. Hence, using (2.1) and the definition of $\mathbf{S}(x, \omega)$ we get

$$\varepsilon(x, \omega) = \mathbf{c}_0^T(\omega)\mathbf{S}(x, \omega), \tag{3.4}$$

where

$$\mathbf{c}_0(\omega) = \left[\begin{array}{cccc} 0 & 0 & \frac{A}{I\mathcal{E}(\omega)} & 0 \end{array}\right]^{\mathrm{T}}. \tag{3.5}$$

We further assume that the strain measurements are corrupted by spatially and temporally white Gaussian noise sequences with mean zero and variance σ. We denote the noise contribution at section x and at time kT by $v(x, k)$, which after discrete Fourier transform gives $V(x, \omega)$. Hence we get noisy measurements $z(x, \omega)$ at frequency ω and at position x as

$$z(x, \omega) = \varepsilon(x, \omega) + V(x, \omega). \tag{3.6}$$

Define the measurement vector $\mathbf{z}(\omega)$, the noise-free strain vector $\boldsymbol{\varepsilon}(\omega)$ and the noise vector $\mathbf{v}(\omega)$ at frequency ω by

$$\mathbf{z}(\omega) = \left[\begin{array}{ccc} z(x_1, \omega) & \ldots & z(x_n, \omega) \end{array}\right]^{\mathrm{T}}, \tag{3.7}$$

$$\boldsymbol{\varepsilon}(\omega) = \left[\begin{array}{ccc} \varepsilon(x_1, \omega) & \ldots & \varepsilon(x_n, \omega) \end{array}\right]^{\mathrm{T}}, \tag{3.8}$$

$$\mathbf{v}(\omega) = \left[\begin{array}{ccc} V(x_1, \omega) & \ldots & V(x_n, \omega) \end{array}\right]^{\mathrm{T}}. \tag{3.9}$$

Combining (2.4), (3.4) and (3.6) and using the definitions (3.7), (3.8) and (3.9) we get

$$\mathbf{z}(\omega) = \mathbf{A}(\omega)\mathbf{c}(\omega) + \mathbf{v}(\omega) = \boldsymbol{\varepsilon}(\omega) + \mathbf{v}(\omega). \tag{3.10}$$

where $\mathbf{A}(\omega)$ is the $n \times 4$ matrix given by

$$\mathbf{A}(\omega) = \left[\begin{array}{cccc} \mathrm{e}^{\gamma_1(\omega)x_1} & \mathrm{e}^{\gamma_2(\omega)x_1} & \mathrm{e}^{-\gamma_1(\omega)x_1} & \mathrm{e}^{-\gamma_2(\omega)x_1} \\ \vdots & \vdots & \vdots & \vdots \\ \mathrm{e}^{\gamma_1(\omega)x_n} & \mathrm{e}^{\gamma_2(\omega)x_n} & \mathrm{e}^{-\gamma_1(\omega)x_n} & \mathrm{e}^{-\gamma_2(\omega)x_n} \end{array}\right]. \tag{3.11}$$

Note that we have introduced an unknown frequency dependent vector $\mathbf{c}(\omega)$, which depends upon the excitation at the boundaries and the gain of the sensors and is given by

$$\mathbf{c}(\omega) = \left[\begin{array}{cccc} \mathbf{c}_1(\omega) & \mathbf{c}_2(\omega) & \mathbf{c}_3(\omega) & \mathbf{c}_4(\omega) \end{array}\right]^{\mathrm{T}} \mathbf{c}_0(\omega). \tag{3.12}$$

Note also that we have assumed the sensors to be identical. From (3.10) we note that the noise-free strain vector $\boldsymbol{\varepsilon}(\omega)$ lies in the column space of $\mathbf{A}(\omega)$, which is

true for all $\mathbf{c}(\omega)$, i.e. the sensor characteristics and the boundary conditions. We also stress that the matrix $\mathbf{A}(\omega)$ is an implicit analytic function of the complex modulus $\mathcal{E}(\omega)$. For notational convenience and for the clarity of understanding, from here onwards we shall use $\mathbf{A}(\mathbf{e}_\omega)$ for $\mathbf{A}(\omega)$. Here we have introduced the frequency dependent real valued parameter vector

$$\mathbf{e}_\omega = \left[\begin{array}{cc} e_r(\omega) & e_i(\omega) \end{array} \right]^{\mathrm{T}}, \tag{3.13}$$

such that

$$\mathcal{E}(\omega) = e_r(\omega) + \mathrm{i} e_i(\omega). \tag{3.14}$$

This notation helps in the sense that we can deal with a real valued parameter vector. Since the boundary conditions are not exactly known, the vector $\mathbf{c}(\omega)$ is also unknown for any frequency ω. For the problem under consideration, $\mathbf{c}(\omega)$ acts as a nuisance parameter vector of dimension four. One approach to obtain an estimate $\hat{\mathbf{e}}_\omega$ of $\mathbf{e}_\omega$ is

$$\hat{\mathbf{e}}_\omega = \arg\min_{\mathbf{e}_\omega} \left\{ \min_{\mathbf{c}(\omega)} \|\mathbf{z}(\omega) - \mathbf{A}(\mathbf{e}_\omega)\mathbf{c}(\omega)\|^2 \right\}. \tag{3.15}$$

This is a separable non-linear least squares problem. It follows from the theory of least squares [13] that after the minimisation with respect to the nuisance parameter vector $\mathbf{c}(\omega)$, the problem simplifies to

$$\hat{\mathbf{e}}_\omega = \arg\min_{\mathbf{e}_\omega} W(\mathbf{e}_\omega), \tag{3.16}$$

$$W(\omega) = \mathbf{z}^*(\omega)\mathbf{P}(\mathbf{e}_\omega)\mathbf{z}(\omega), \tag{3.17}$$

where $\mathbf{P}(\mathbf{e}_\omega)$ denotes the projection operator onto the null space of $\mathbf{A}^*(\mathbf{e}_\omega)$, given by

$$\mathbf{P}(\mathbf{e}_\omega) = \mathbf{I}_n - \mathbf{A}(\mathbf{e}_\omega)\mathbf{A}^\dagger(\mathbf{e}_\omega). \tag{3.18}$$

Here we have denoted the unity matrix of order n by $\mathbf{I}_n$. Further, the pseudo-inverse $\mathbf{A}^\dagger(\mathbf{e}_\omega)$ of $\mathbf{A}(\mathbf{e}_\omega)$ is determined by the relation

$$\mathbf{A}^\dagger(\mathbf{e}_\omega) = \left[\mathbf{A}^*(\mathbf{e}_\omega)\mathbf{A}(\mathbf{e}_\omega)\right]^{-1} \mathbf{A}^*(\mathbf{e}_\omega), \tag{3.19}$$

where we denote the conjugate-transpose of a matrix X by X^*. Note that for the relation (3.19) to hold, we need to assume $\mathbf{A}(\mathbf{e}_\omega)$ to be full rank, i.e. $\mathbf{A}(\mathbf{e}_\omega)$ is of rank 4 for all ω. Under certain circumstances to be clarified later, it is not always possible to justify this assumption. We shall return to this aspect later in this paper.

Since it is known that the noise-free strain vector $\boldsymbol{\varepsilon}(\omega)$ lies in the column space of $\mathbf{A}(\mathbf{e}_\omega)$, it is reasonable to choose $\hat{\mathbf{e}}_\omega$ such that the orthogonal projection of the strain vector $\mathbf{z}(\omega)$ onto the null-space of $\mathbf{A}^*(\mathbf{e}_\omega)$ is minimised. This is precisely what is done in (3.16) when we minimise $W(\mathbf{e}_\omega)$ in (3.17) with respect to $\mathbf{e}_\omega$. For the estimator $\hat{\mathbf{e}}_\omega$ given by (3.16), we have the following main result.

Theorem: Denote the true parameter vector at frequency ω by $\mathbf{e}_{\omega 0}$. Then for any two discrete frequencies ω_j and ω_k as in (3.1), and for a large signal to noise ratio it holds that

$$E\left\{ \left(\hat{\mathbf{e}}_{\omega_j} - \mathbf{e}_{\omega_j 0} \right) \left(\hat{\mathbf{e}}_{\omega_k} - \mathbf{e}_{\omega_k 0} \right)^{\mathrm{T}} \right\} = \frac{\sigma}{h(\omega_j)} \delta_{j,k}\, \mathbf{I}_2, \quad 0 < j, k < N/2, \tag{3.20}$$

where $\delta_{j,k}$ denotes the Kronecker delta function, and

$$h(\omega) = 2\boldsymbol{\varepsilon}^*(\omega)\mathbf{A}^{\dagger *}(\mathbf{e}_{\omega 0})\mathbf{A}_r^*(\mathbf{e}_{\omega 0})\mathbf{P}(\mathbf{e}_{\omega 0})\mathbf{A}_r(\mathbf{e}_{\omega 0})\mathbf{A}^{\dagger}(\mathbf{e}_{\omega 0})\boldsymbol{\varepsilon}(\omega) \quad (3.21)$$

$$= 2\mathbf{c}^*(\omega)\mathbf{A}_r^*(\mathbf{e}_{\omega 0})\mathbf{P}(\mathbf{e}_{\omega 0})\mathbf{A}_r(\mathbf{e}_{\omega 0})\mathbf{c}(\omega). \quad (3.22)$$

The notation $\mathbf{A}_r(\mathbf{e}_\omega)$ is defined as

$$\mathbf{A}_r(\mathbf{e}_\omega) = \frac{\partial \mathbf{A}(\mathbf{e}_\omega)}{\partial e_r(\omega)}. \quad (3.23)$$

Proof: See Appendix A. ■

We stress that the signal to noise ratio in practice is large. Hence, this assumption in the theorem is reasonable. A similar analysis has been carried out in [11], where extensional wave propagation experiments are considered. The analysis to be carried out in this paper is simpler and gives a more compact final expression. This enables us also to have a deeper insight into the statistical properties of the estimator. We stress that the same expressions are also valid for any other separable non-linear least squares problem of the same type.

Since the the vector $\mathbf{c}(\omega)$ is unknown in practical experiments, the form (3.21) is more useful from application point of view. Some issues related to the computational aspects are discussed in the next section. As the consequence of the above theorem, we have the following implications.

- The estimate of the complex modulus at a particular frequency is uncorrelated with the same at any other frequency.
- At a particular frequency, the estimate of the real part of the complex modulus is uncorrelated with the estimate of the imaginary part.
- The estimate of the real part of the complex modulus has the same variance as the estimate of the imaginary part, although their absolute magnitudes may be of different orders.
- Note from (3.21) that $h(\omega)$ is directly proportional to the signal energy and hence from (3.20) we conclude that the variance of the real part (or the imaginary part) of the complex modulus is inversely proportional to the signal to noise ratio.
- The estimation accuracy is an implicit function of the sensor locations and the type of excitation. It is directly related to the excitation signal through $\mathbf{c}(\omega)$, see (3.22), while it depends upon the sensor locations through $\mathbf{A}(\mathbf{e}_\omega)$.

4 Numerical issues

In the previous section, we asssumed that the matrix $\mathbf{A}(\mathbf{e}_\omega)$ to be full rank for the expression (3.19) to hold. This is not a restrictive assumption in general, in the sense that each of the single dimensional subspaces spanned by the invidual columns of $\mathbf{A}(\mathbf{e}_\omega)$ are well seperated from each other. However, the matrix $\mathbf{A}(\mathbf{e}_\omega)$

is often badly scaled so that its condition number is significantly large. Under this condition it is likely to introduce significant numerical errors while computing $\mathbf{A}^{\dagger}(\mathbf{e}_{\omega})$. This may lead to two types of problems in what we have presented so far. Firstly, it is often likely to do some rounding errors during the optimisation in (3.16), so that we arrive at an $\hat{\mathbf{e}}_{\omega}$ which may differ drastically from $\mathbf{e}_{\omega 0}$. Secondly, during the computation of the variance of the estimates using (3.20) and (3.21), we may get a wrong value. This problem is more prominent at higher frequencies, since the condition number of $\mathbf{A}(\mathbf{e}_{\omega})$ increases with the frequency.

As mentioned before, this phenomenon can be attributed to the fact that the matrix $\mathbf{A}(\mathbf{e}_{\omega})$ is often badly scaled. To explain the idea, let us refer to the Figure 2. We note here that the real part of the propagation function γ_1 increases rapidly with increasing frequency. Assuming the value of x increases towards right, the first column of $\mathbf{A}(\mathbf{e}_{\omega})$, thus have a significantly large norm compared to the norms of the other columns, see (3.11). Similarly, with the increase in the frequency, the norm of the second column of $\mathbf{A}(\mathbf{e}_{\omega})$ also increases to a large value compared to the norm of the third and the fourth column. In fact, the norms of the third column and the fourth column of $\mathbf{A}(\mathbf{e}_{\omega})$ are decreasing functions of frequency. Hence the condition number of $\mathbf{A}(\mathbf{e}_{\omega})$ grows very fast with the frequency.

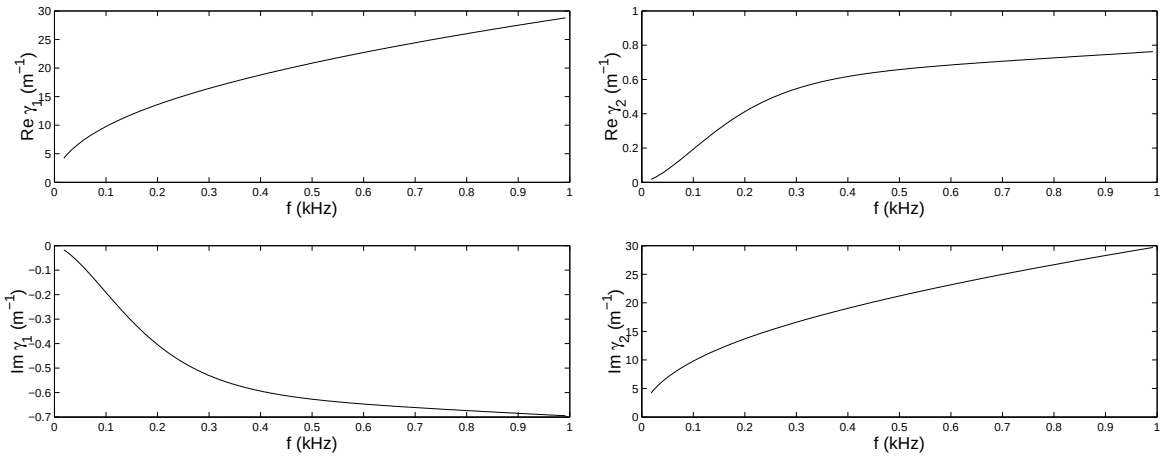

(a) $\gamma_1(\omega)$ (b) $\gamma_2(\omega)$

Figure 2: The wave propagation functions plotted as a function of frequency.

To cope up with the problem mentioned here, it is thus necessary to scale the columns of $\mathbf{A}(\mathbf{e}_{\omega})$ properly, so that the norms of the individual columns of $\mathbf{A}(\mathbf{e}_{\omega})$ are of comparable magnitude. In this aim we introduce the diagonal matrix

$$\mathbf{D}(\omega) = \begin{bmatrix} \mathrm{e}^{-\gamma_1(\omega)(L+x_0)} & 0 & 0 & 0 \\ 0 & \mathrm{e}^{-\gamma_2(\omega)(L+x_0)} & 0 & 0 \\ 0 & 0 & \mathrm{e}^{\gamma_1(\omega)x_0} & 0 \\ 0 & 0 & 0 & \mathrm{e}^{\gamma_2(\omega)x_0} \end{bmatrix}, \tag{4.1}$$

where x_0 denote the position of section A of the bar segment under consideration

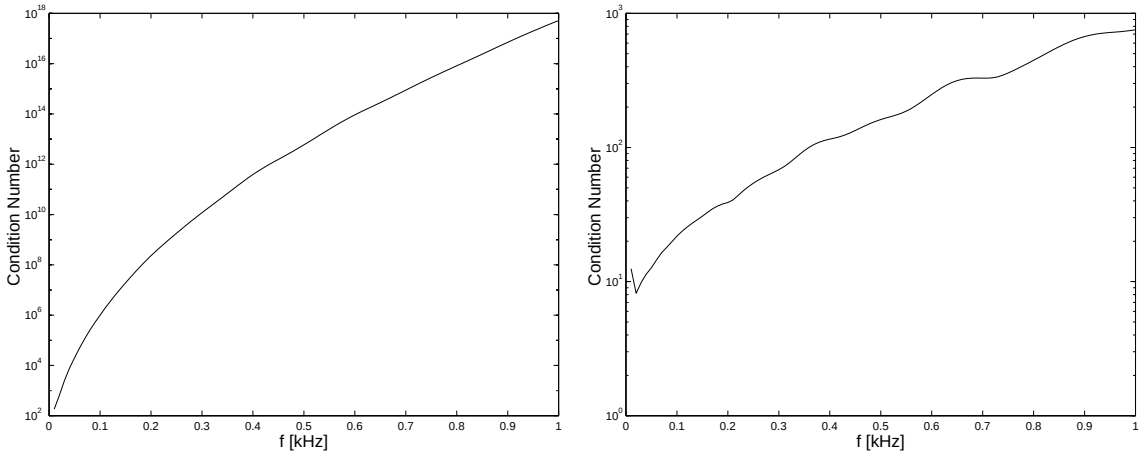

(a) $\mathbf{A}(\mathbf{e}_\omega)$ (b) $\mathbf{A_s}(\mathbf{e}_\omega)$

Figure 3: The condition numbers of $\mathbf{A}(\mathbf{e}_\omega)$ and $\mathbf{A_s}(\mathbf{e}_\omega)$ plotted as a function of frequency.

(see Figure 1). We scale $\mathbf{A}(\mathbf{e}_\omega)$ as

$$\mathbf{A_s}(\mathbf{e}_\omega) = \mathbf{A}(\mathbf{e}_\omega)\mathbf{D}(\omega). \tag{4.2}$$

The matrix $\mathbf{A_s}(\mathbf{e}_\omega)$ is well behaved and has good numerical properties. See Figure 3 for a comparison of the condition numbers of $\mathbf{A_s}(\mathbf{e}_\omega)$ and $\mathbf{A}(\mathbf{e}_\omega)$. Note the column space of $\mathbf{A}(\mathbf{e}_\omega)$ is the same as the column space of $\mathbf{A_s}(\mathbf{e}_\omega)$. We have the following lemma, which can be seen as a guideline to use $\mathbf{A_s}(\mathbf{e}_\omega)$ effectively.

Lemma: Let $\mathbf{P_s}(\mathbf{e}_\omega)$ be the projection operator onto the nullspace of $\mathbf{A_s}^*(\mathbf{e}_\omega)$. Then

$$W(\omega) = \mathbf{z}^*(\omega)\mathbf{P_s}(\mathbf{e}_\omega)\mathbf{z}(\omega), \tag{4.3}$$

$$h(\omega) = 2\boldsymbol{\varepsilon}^*(\omega)\mathbf{A_s}^{\dagger *}(\mathbf{e}_{\omega 0})\mathbf{D}^*(\omega)\mathbf{A}_r^*(\mathbf{e}_{\omega 0})\mathbf{P_s}(\mathbf{e}_{\omega 0})\mathbf{A}_r(\mathbf{e}_{\omega 0})\mathbf{D}(\omega)\mathbf{A_s}^\dagger(\mathbf{e}_{\omega 0})\boldsymbol{\varepsilon}(\omega). \tag{4.4}$$

Proof: See Appendix. ■

Note that in (4.3) and (4.4) $\mathbf{A}^\dagger(\mathbf{e}_\omega)$ and $\mathbf{P}(\mathbf{e}_\omega)$ never appear. This is how we can reduce the probability of making numerical errors. We stress that the expressions (4.3) and (4.4) are also valid for any full rank $\mathbf{D}(\omega)$, among which (4.1) is a special case. Hence $\mathbf{D}(\omega)$ in (4.2) can be replaced by any other *preconditioner* matrix without affecting (4.3) and (4.4). Using the expression (4.3) it is easy to verify that the estimated complex modulus is independent of the origin of the co-ordinate system (which is a mandatory requirement). To see this we refer to (3.11) where we can verify that any change in origin is precisely reflected as the matrix $\mathbf{A}(\mathbf{e}_\omega)$ being post-multiplied by a full rank square matrix.

It can be seen in Figure 3(b) that the condition number of the scaled matrix $\mathbf{A_s}(\mathbf{e}_\omega)$ is an increasing function of ω. To keep rounding errors in control, it is recomended to use QR factorisation [5] of $\mathbf{A_s}(\mathbf{e}_\omega)$ while computing its pseudoinverse $\mathbf{A_s}^\dagger(\mathbf{e}_\omega)$ and the projection operator $\mathbf{P_s}(\mathbf{e}_\omega)$ onto the nullspace of $\mathbf{A_s}^*(\mathbf{e}_\omega)$. In what follows

we shall omit the arguments of the matrices for notational convenience. Consider the QR factorisation of $\mathbf{A_s}$ is given by

$$\mathbf{A_s} = QR = \begin{bmatrix} Q_1 & Q_2 \end{bmatrix} \begin{bmatrix} R_1 \\ 0 \end{bmatrix}, \tag{4.5}$$

where Q is a $n \times n$ orthogonal matrix splitted into blocks Q_1 $(n \times 4)$ and Q_2 $(n \times n-4)$, and R is an upper triangular matrix which has a 4×4 upper triangular block R_1. Note that

$$\mathbf{A_s} = Q_1 R_1 \tag{4.6}$$

Thus, we have

$$\mathbf{A_s}^\dagger = \left[\mathbf{A_s}^* \mathbf{A_s}\right]^{-1} \mathbf{A_s}^* = \left[R_1^* Q_1^* Q_1 R_1\right]^{-1} R_1^* Q_1^* = R_1^{-1} Q_1^*. \tag{4.7}$$

Note that we used $Q_1^* Q_1 = \mathbf{I}_4$ in the last equality, which follows from the orthogonality of Q. Hence $\mathbf{P_s}$ is given by

$$\mathbf{P_s} = \mathbf{I}_n - \mathbf{A_s}\mathbf{A_s}^\dagger = \mathbf{I}_n - Q_1 R_1 R_1^{-1} Q_1^* = \mathbf{I}_n - Q_1 Q_1^* = Q_2 Q_2^*. \tag{4.8}$$

The last equality follows from the orthogonality of Q. Hence by (3.17) we get

$$W(\mathbf{e}_\omega) = \|Q_2^* \mathbf{z}(\omega)\|^2. \tag{4.9}$$

Hence (4.3) and (4.4) along with (4.7) and (4.9) give numerically sound ways to compute all the relevant quantities.

5 Numerical simulation study

The experiment described in the Section 1 and the non-parametric identification technique in Section 3 were considered in a Monte Carlo simulation study in order to investigate the validity of the accuracy expression given by the theorem in Section 3. Data for the wave propagation constants were generated using two standard linear solid models in parallel [2], for which the complex modulus is given by

$$\mathcal{E}(\omega) = \frac{M}{2}\left\{\frac{1+\omega\tau_1}{1+\omega\tau_2} + \frac{1+\omega\tau_3}{1+\omega\tau_4}\right\}, \tag{5.1}$$

where we have taken $M = 2.231$ GPa, $\tau_1 = 765.2$ μs, $\tau_2 = 504.8$ μs, $\tau_3 = 95.6$ μs and $\tau_4 = 75.53$ μs. With this choice of viscoelastic parameters, the material model applies to the dynamic behaviour of polypropylene (PP), for which the density $\rho = 915$ kg/m^3 and the Poission's ratio $\nu = 0.44$. We have $\psi = 3.2$ for a circular cross-section. The boundary conditions for the experimental set up are as follows.

$$M(x_0 + L, t) = f(t), \quad M(x_0, t) = 0, \quad w(x_0, t) = w(x_0 + L, t) = 0. \tag{5.2}$$

The exciting bending moment pulse $f(t)$ at the right end of the bar was chosen so that sufficient excitation for all considered frequencies were provided. The excitation pulse and its frequency response are shown in Figure 4. The vector $\mathbf{c}(\omega)$ in (3.10) is determined by inserting the boundary conditions (5.2) into (2.4) and (3.5). The length of the bar was $L = 1.5$ m, the number of data points was

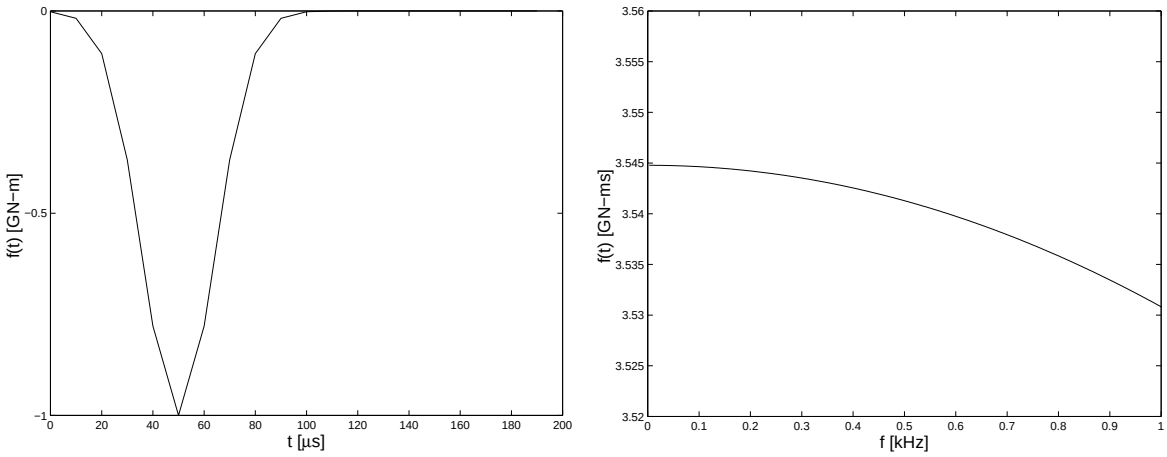

(a) (b)

Figure 4: The excitation pulse (a) and its frequency response in the region of interest (b) used as the boundary condition in the simulations.

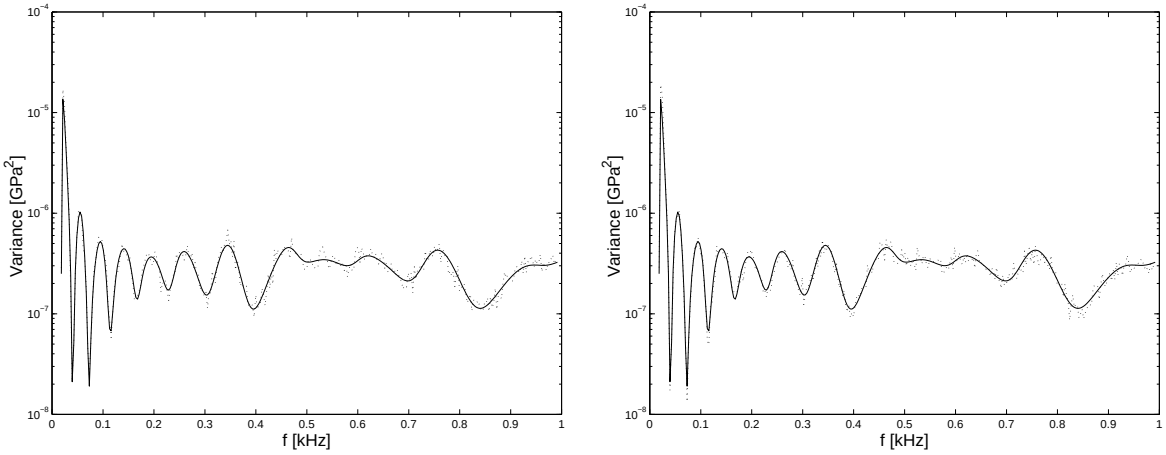

(a) Variance of $\hat{e}_r$ (b) Variance of $\hat{e}_i$

Figure 5: Comparison between the analytitical variance (solid line) with the numerical variance (dotted line) from the simulations. (a) Variance of $\hat{e}_r$. (b) Variance of $\hat{e}_i$.

$N = 2^{15}$ and the sampling interval was $T = 50$ μs. The positions $\{x_i\}_{i=1}^n$ of the sensors were taken exactly as in the experiment described by Figure 1. They are given by

$$\left\{ \begin{array}{cccccccc} 0.102 & 0.348 & 0.468 & 0.685 & 0.870 & 1.003 & 1.147 & 1.300 \end{array} \right\}, \qquad (5.3)$$

where the co-ordinates are expressed in meter. The simulated strains were affected by noise in time domain and estimates of the complex elastic modulus were obtained using (3.16). This procedure of noise addition and estimation was repeated 100 times with different noise realisations. The ratio of the noise standard deviation to the maximum absolute value of the true strain was of the order 10^{-2}.

The standard deviations of the estimates from the 100 simulated experiments were compared to the corresponding theoretical values given by (3.21). The result of such a comparison is shown in Figure 5. The numerical variance of the estimates can be seen to be well in accordance with the analytical variance predicted by (3.20).

6 Experimental results

The recorded analog strain signals were sampled at 20 kHz and the corresponding value of $T = 5$ μs . The number of samples collected from each channel was 60000. The signals were padded with zeros to make $N = 2^{16}$. This zero padding helps us to increase the resolution in frequency domain and with this choice of N we can use the computationally efficient radix-2 Fast Fourier Transform algorithm [12] to compute DFT. With these values of N and T we have a resolution of 0.3 Hz in the frequency domain. At the beginning of the interval, the tested beam was at rest, and at the end the signals were reduced almost to the level of the noise. This ensures that the signals could be transferred to the frequency domain by the FFT algorithm without the use of any window technique.

As only one data set was originally available, but acquired with reasonably large sampling rate, the data vectors $\{\mathbf{z}(\omega_k)\}_{k=0}^{N/2}$ with tightly spaced frequencies $\{\omega_k\}_{k=0}^{N-1}$ were available. We assume the effect of systematic variation of the complex modulus $\mathcal{E}(\omega)$ on the variation of $\hat{\mathbf{e}}_\omega$ is small compared to the noise effect within a short frequency interval of 3 Hz. This assumption can be justified later in Figure 6. From the proposition 1 in the appendix we note that the noise vectors $\mathbf{v}(\omega_j)$ and $\mathbf{v}(\omega_k)$ are independent if $k \neq j$. Based on these observation and assumption, 'ten independent experiments' were obtained for each separate frequency by using data from ten neighbouring frequencies as well.

The results of the identification is plotted in Figure 6, where the variation of the real part and the imaginary part of the complex modulus as a function of frequency is shown. The value of the complex modulus at each frequency is obtained by averaging the results of 'ten experiments'. The real and the imaginary parts of the parametric complex modulus (5.1) used in the numerical simulation study with the parameter values mentioned in the previous section is compared with those obtained from the experiments in Figure 6. We see that the parametric complex modulus (5.1) resembles closely to the experimental complex modulus. We therefore can use the results of the simulation study as a benchmark. In order to check the validity of the expressions given by (3.20), (3.21) and (3.22), the analytical variance was compared with the sample variance obtained from ten independent experiments. The result of such a comparison is shown in Figure 7.

Note that the noise variance σ and the true strain $\boldsymbol{\varepsilon}(\omega)$ are required to compute the analytical variance, see (3.20) and (3.21). These are unknown. While computing the theoretical variance, $\boldsymbol{\varepsilon}(\omega)$ was approximated by $\mathbf{z}(\omega)$, which is justified since the signal to noise ratio is high. Note also that, even if the noise variance is unknown, the theoretical variance (3.20) obtained using an arbitrary value of σ

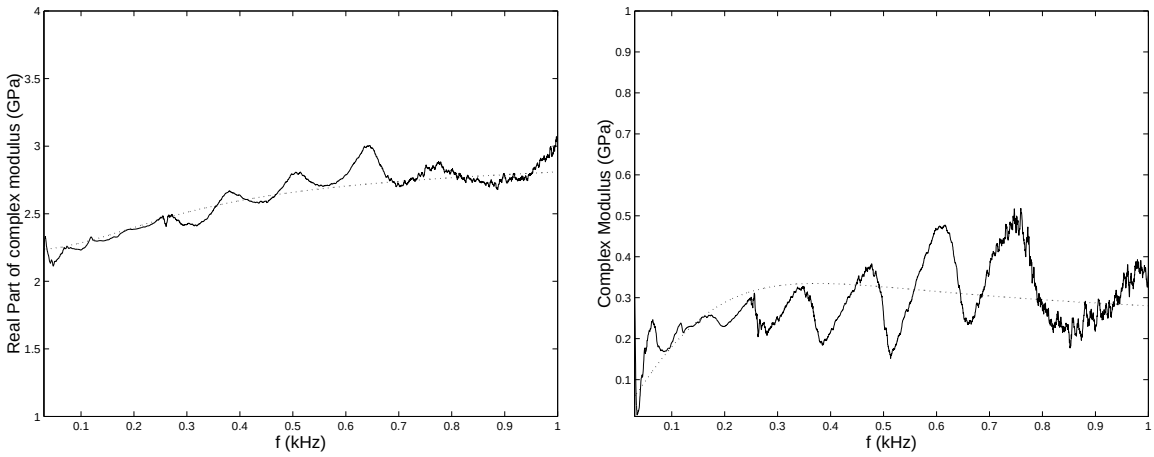

(a) $\hat{e}_r$ (b) $\hat{e}_i$

Figure 6: Complex mudulus obtained from the experiments (solid line) and the parametric complex modulus (dotted line) given by (5.1).

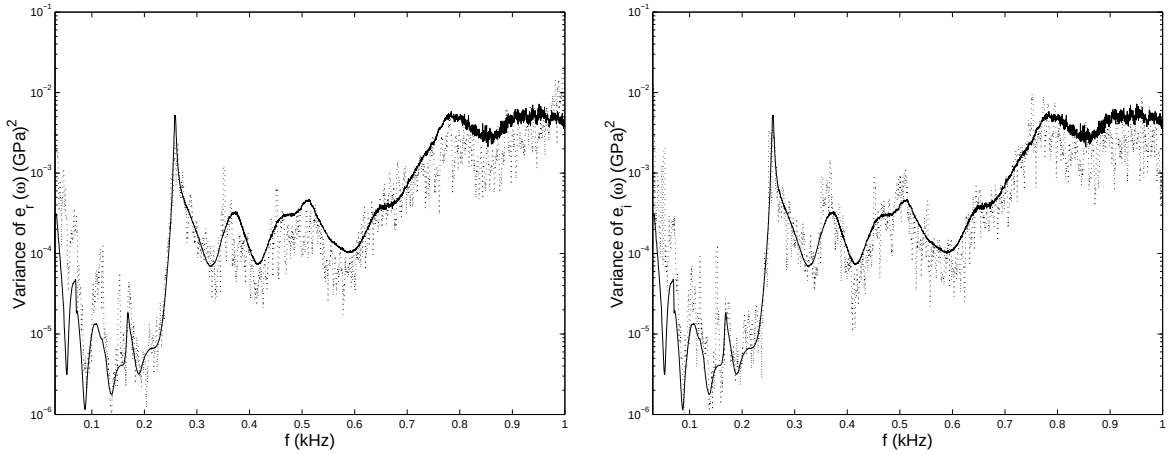

(a) Variance of $\hat{e}_r$ (b) Variance of $\hat{e}_i$

Figure 7: Comparison between the analytical variance (solid line) to the experimental variance (dotted line). (a) Variance of $\hat{e}_r$. (b) Variance of $\hat{e}_i$.

is directly proportional to the actual variance of the estimates, which should be reflected as a constant difference in a semilog scale. The value of σ used in the calculation of the theoretical variance (3.20) is 2×10^{-8}. It can be seen in Figure 7 that the theoretical prediction using (3.20), (3.21) and (3.22) is very well in accordance with the results obtained from the experiments. Let us now compare the results in Figure 7 with the results obtained from the simulation study in Figure 6. We can notice in Figure 7 that the individual variances of the complex modulus estimates obtained from the experiments increase significantly with frequency. This is not the case in Figure 6, where the results from numerical simulation study are depicted. This observation indicates the fact that the signal to noise ratio of

the experimental data is low at high frequencies.

7 Conclusions

In this paper, we have presented a method of obtaining the complex modulus of a linearly viscoelastic material using flexural wave propagation experiments on a bar specimen. The numerical problems associated with the implementation of the algorithms are treated in detail. Some methods to remedy the numerical problems are suggested. The covariance matrix of the complex modulus estimate is derived. The validity of the analytical expression is confirmed using a numerical simulation study and also from real experimental data. The experimental observations and simulation studies reveal that the expression given by (3.20), (3.21) and (3.22) can be used as a guideline to design the experiment to achieve the best possible accuracy. A comparison between the results from the numerical simulation study and the experimental observations reveals that the excitation at higher frequencies may not be of sufficient strength in the set up given in Figure 1.

A Proof of the theorem

In order to prove the theorem we need the following propositions. The first proposition characterises the noise vector $\mathbf{v}(\omega)$.

Proposition 1: The noise vector $\mathbf{v}(\omega)$ defined in (3.9) satisfies

$$\begin{aligned} E\mathbf{v}(\omega_k) &= 0 \quad \forall k & \text{(A.1)} \\ E\mathbf{v}(\omega_l)\mathbf{v}^{\mathrm{T}}(\omega_k) &= 0, \quad \forall l,k \text{ such that } 0 < l,k < N/2, & \text{(A.2)} \\ E\mathbf{v}(\omega_l)\mathbf{v}^{*}(\omega_k) &= \delta_{l,k}\mathbf{I}_n, \quad \forall l,k \text{ such that } 0 < l,k < N/2. & \text{(A.3)} \end{aligned}$$

Proof: From the definition of DFT, the frequency response $V(x,\omega)$ of the sequence $\{v(x,k)\}_{k=0}^{N-1}$ is given by

$$V(x,\omega) = \frac{1}{\sqrt{N}} \sum_{k=0}^{N-1} v(x,k) \mathrm{e}^{-\mathrm{i}\frac{2\pi}{N}k}. \tag{A.4}$$

By the zero mean assumption on $v(x,k)$, (A.1) follows from (A.4). Now from (A.4) we have

$$\begin{aligned} EV(x_i,\omega_k)V(x_j,\omega_l) &= \frac{1}{N} \sum_{p=0}^{N-1} \sum_{q=0}^{N-1} Ev(x_i,p)v(x_j,q) \mathrm{e}^{-\mathrm{i}\frac{2\pi}{N}[pk+ql]} \\ = \quad \sigma\delta_{i,j} \frac{1}{N} \sum_{p=0}^{N-1} \sum_{q=0}^{N-1} \delta_{p,q} \mathrm{e}^{-\mathrm{i}\frac{2\pi}{N}[pk+ql]} &= \sigma\delta_{i,j} \frac{1}{N} \sum_{p=0}^{N-1} \mathrm{e}^{-\mathrm{i}\frac{2\pi}{N}p[k+l]} \\ = \quad 0, \quad 0 < k,l < N/2. & \qquad \text{(A.5)} \end{aligned}$$

Similarly

$$EV(x_i,\omega_k)V^{*}(x_j,\omega_l) = \frac{1}{N} \sum_{p=0}^{N-1} \sum_{q=0}^{N-1} Ev(x_i,p)v(x_j,q) \mathrm{e}^{-\mathrm{i}\frac{2\pi}{N}[pk-ql]}$$

$$
\begin{aligned}
&= \sigma\delta_{i,j}\frac{1}{N}\sum_{p=0}^{N-1}\sum_{q=0}^{N-1}\delta_{p,q}\mathrm{e}^{-\mathrm{i}\frac{2\pi}{N}[pk-ql]} = \sigma\delta_{i,j}\frac{1}{N}\sum_{p=0}^{N-1}\mathrm{e}^{-\mathrm{i}\frac{2\pi}{N}p[k-l]} \\
&= \sigma\delta_{i,j}\delta_{k,l}, \quad 0 < k, l < N/2. \qquad \text{(A.6)}
\end{aligned}
$$

Thus, (A.2) follows directly from (3.9) using (A.5), while we get (A.3) from (3.9) and (A.6). ■

By the above proposition we conclude that $\mathbf{v}(\omega)$ is a complex Gaussian random variable. We shall use the following proposition concerning the expectation of the quadratic forms of the complex Gaussian random vectors.

Proposition 2: Let $\mathbf{x}$ be a complex value deterministic vector of the same dimension as $\mathbf{v}(\omega)$. Let R and S are matrices of compatible dimension such that $\mathbf{x}^*R\mathbf{x} = \mathbf{x}^*S\mathbf{x} = 0$. Then

$$
\begin{aligned}
&E[\mathbf{x}+\mathbf{v}(\omega)]^*R[\mathbf{x}+\mathbf{v}(\omega)][\mathbf{x}+\mathbf{v}(\omega)]^*S[\mathbf{x}+\mathbf{v}(\omega)] \\
&\qquad = \sigma\mathbf{x}^*[RS+SR]\mathbf{x} + \sigma^2[tr(S)\mathrm{tr}(R) + \mathrm{tr}(SR)], \qquad \text{(A.7)}
\end{aligned}
$$

where $\mathrm{tr}(X)$ denote the trace of the matrix X.

Proof: We shall omit the argument ω of $\mathbf{v}(\omega)$ for convenience and denote the conjugate of $\mathbf{v}$ by $\overline{\mathbf{v}}$. Using the assumptions we get

$$
\begin{aligned}
&E[\mathbf{x}+\mathbf{v}]^*R[\mathbf{x}+\mathbf{v}][\mathbf{x}+\mathbf{v}]^*S[\mathbf{x}+\mathbf{v}] \\
= \;& E[\mathbf{x}^*R\mathbf{v}+\mathbf{v}^*R\mathbf{x}+\mathbf{v}^*R\mathbf{v}]E[\mathbf{x}^*S\mathbf{v}+\mathbf{v}^*S\mathbf{x}+\mathbf{v}^*S\mathbf{v}]. \qquad \text{(A.8)}
\end{aligned}
$$

Next we use the properties of $\mathbf{v}$ and note that the third order moments of a zero mean Gaussian random vector vanish. Keeping only the nonzero terms we have

$$
\begin{aligned}
&E[\mathbf{x}+\mathbf{v}]^*R[\mathbf{x}+\mathbf{v}][\mathbf{x}+\mathbf{v}]^*S[\mathbf{x}+\mathbf{v}] \\
= \;& E[\mathbf{x}^*R\mathbf{v}\mathbf{v}^*S\mathbf{x}+\mathbf{x}^*S\mathbf{v}\mathbf{v}^*R\mathbf{x}+\mathbf{v}^*S\mathbf{v}\mathbf{v}^*R\mathbf{v}] \\
= \;& \sigma\mathbf{x}^*[RS+SR]\mathbf{x} + E[\mathbf{v}^*S\mathbf{v}\mathbf{v}^*R\mathbf{v}], \qquad \text{(A.9)}
\end{aligned}
$$

where we have used (A.3) in the last eqality. For the last term, by the property of jointly Gaussian random variables [9] we get

$$
\begin{aligned}
&E[\mathbf{v}^*S\mathbf{v}\mathbf{v}^*R\mathbf{v}] \\
= \;& E[\mathbf{v}^*S\mathbf{v}]E[\mathbf{v}^*R\mathbf{v}] + E[\mathbf{v}^*SE\{\mathbf{v}\mathbf{v}^*\}R\mathbf{v}] + E[\mathbf{v}^*SE\{\mathbf{v}\mathbf{v}^{\mathrm{T}}\}R^{\mathrm{T}}\overline{\mathbf{v}}] \\
= \;& \mathrm{tr}[SE\mathbf{v}\mathbf{v}^*]\mathrm{tr}[RE\mathbf{v}\mathbf{v}^*] + \sigma E[\mathbf{v}^*SR\mathbf{v}] \\
= \;& \sigma^2[\mathrm{tr}(S)\mathrm{tr}(R) + \mathrm{tr}(SR)]. \qquad \text{(A.10)}
\end{aligned}
$$

Note that we used (A.3) in the last equality and (A.2) in the second equality. Thus, combining (A.9) and (A.10) we get (A.7). ■

At this point, let us introduce the following notations.

$$
\mathbf{A}_r(\mathbf{e}_\omega) \;=\; \frac{\partial\mathbf{A}(\mathbf{e}_\omega)}{\partial e_r(\omega)} \qquad \text{(A.11)}
$$

$$\mathbf{A}_i(\mathbf{e}_\omega) = \frac{\partial \mathbf{A}(\mathbf{e}_\omega)}{\partial e_i(\omega)} \tag{A.12}$$

$$\mathbf{A}_{rr}(\mathbf{e}_\omega) = \frac{\partial^2 \mathbf{A}(\mathbf{e}_\omega)}{\partial e_r^2(\omega)} \tag{A.13}$$

$$\mathbf{A}_{ii}(\mathbf{e}_\omega) = \frac{\partial^2 \mathbf{A}(\mathbf{e}_\omega)}{\partial e_i^2(\omega)} \tag{A.14}$$

$$\mathbf{A}_{ri}(\mathbf{e}_\omega) = \frac{\partial^2 \mathbf{A}(\mathbf{e}_\omega)}{\partial e_r(\omega)\partial e_i(\omega)} \tag{A.15}$$

Similar notations will be used to express the derivatives of for any other functions of $\mathbf{e}_\omega$. Applying Cauchy-Riemann's conditions for analytic functions [3] to $\mathbf{A}(\mathbf{e}_\omega)$ we get

$$\mathbf{A}_i(\mathbf{e}_\omega) = \mathrm{i}\mathbf{A}_r(\mathbf{e}_\omega) \tag{A.16}$$

$$\mathbf{A}_{rr}(\mathbf{e}_\omega) = -\mathbf{A}_{ii}(\mathbf{e}_\omega) = -\mathrm{i}\mathbf{A}_{ri}(\mathbf{e}_\omega) \tag{A.17}$$

Thus it is sufficient to know and in order to find the other derivatives of first and second order. We have the following results, which we shall not prove but refer to [6], [14].

$$\mathbf{P}_r(\mathbf{e}_\omega) = -\left[\mathbf{P}(\mathbf{e}_\omega)\mathbf{A}_r(\mathbf{e}_\omega)\mathbf{A}^\dagger(\mathbf{e}_\omega)\right] - \left[\mathbf{P}(\mathbf{e}_\omega)\mathbf{A}_r(\mathbf{e}_\omega)\mathbf{A}^\dagger(\mathbf{e}_\omega)\right]^* \tag{A.18}$$

$$\mathbf{P}_i(\mathbf{e}_\omega) = -\left[\mathbf{P}(\mathbf{e}_\omega)\mathbf{A}_i(\mathbf{e}_\omega)\mathbf{A}^\dagger(\mathbf{e}_\omega)\right] - \left[\mathbf{P}(\mathbf{e}_\omega)\mathbf{A}_i(\mathbf{e}_\omega)\mathbf{A}^\dagger(\mathbf{e}_\omega)\right]^* \tag{A.19}$$

Using these results we shall prove the next proposition, which will be required to derive the hessian of the cost function in (3.17).

Proposition 3: The second order derivatives of the projection operator $\mathbf{P}(\mathbf{e}_\omega)$ satisfies the following.

$$\begin{aligned}
\boldsymbol{\varepsilon}^*(\omega)\mathbf{P}_{rr}(\mathbf{e}_\omega)\boldsymbol{\varepsilon}(\omega) &= \boldsymbol{\varepsilon}^*(\omega)\mathbf{P}_{ii}(\mathbf{e}_\omega)\boldsymbol{\varepsilon}(\omega) \\
&= 2\boldsymbol{\varepsilon}^*(\omega)\mathbf{A}^{\dagger *}\mathbf{A}_r^*(\mathbf{e}_\omega)\mathbf{P}(\mathbf{e}_\omega)\mathbf{A}_r(\mathbf{e}_\omega)\mathbf{A}^\dagger(\mathbf{e}_\omega)\boldsymbol{\varepsilon}(\omega) \\
&= 2\mathbf{c}^*(\omega)\mathbf{A}_r^*(\mathbf{e}_\omega)\mathbf{P}(\mathbf{e}_\omega)\mathbf{A}_r(\mathbf{e}_\omega)\mathbf{c}(\omega), \qquad \text{(A.20)} \\
\boldsymbol{\varepsilon}^*(\omega)\mathbf{P}_{ri}(\mathbf{e}_\omega)\boldsymbol{\varepsilon}(\omega) &= 0 \qquad \text{(A.21)}
\end{aligned}$$

Proof: In this proof, the arguments of the matrices will be omitted for convenience. Since $\mathbf{PA} = 0$, we have using (3.10)

$$\begin{aligned}
\boldsymbol{\varepsilon}^*\left[\mathbf{P}\mathbf{A}_i\mathbf{A}^\dagger\right]_i &= \mathbf{c}^*\mathbf{A}^*\left[\mathbf{P}_i\mathbf{A}_i\mathbf{A}^\dagger + \mathbf{P}\mathbf{A}_{ii}\mathbf{A}^\dagger + \mathbf{P}\mathbf{A}_i\left(\mathbf{A}^\dagger\right)_i\right]\mathbf{A}\mathbf{c} \\
&= \mathbf{c}^*\mathbf{A}^*\mathbf{P}_i\mathbf{A}_i\mathbf{A}^\dagger\mathbf{A}\mathbf{c} \\
&= -\mathbf{c}^*\mathbf{A}^*\left[\mathbf{P}\mathbf{A}_i\mathbf{A}^\dagger + \mathbf{A}^{\dagger *}\mathbf{A}_i^*\mathbf{P}\right]\mathbf{A}_i\mathbf{c} \\
&= -\mathbf{c}^*\mathbf{A}^*\mathbf{A}^{\dagger *}\mathbf{A}_i^*\mathbf{P}\mathbf{A}_i\mathbf{c} \\
&= -\mathbf{c}^*\mathbf{A}_i^*\mathbf{P}\mathbf{A}_i\mathbf{c} \qquad \text{(A.22)}
\end{aligned}$$

Note that we have used (A.19) in the third equality. Since $\mathbf{P}$ is a Hermitian matrix, the right hand side of (A.22) is a real valued scalar. Hence by (A.12), (A.19) and (A.22) we get

$$\begin{aligned}
\boldsymbol{\varepsilon}^*\mathbf{P}_{ii}\boldsymbol{\varepsilon} &= -\boldsymbol{\varepsilon}^*\left[\mathbf{P}\mathbf{A}_i\mathbf{A}^\dagger\right]_i\boldsymbol{\varepsilon} - \left\{\boldsymbol{\varepsilon}^*\left[\mathbf{P}\mathbf{A}_i\mathbf{A}^\dagger\right]_i\boldsymbol{\varepsilon}\right\}^* \\
&= 2\mathbf{c}^*\mathbf{A}_i^*\mathbf{P}\mathbf{A}_i\mathbf{c} = 2\mathbf{c}^*\mathbf{A}_r^*\mathbf{P}\mathbf{A}_i\mathbf{c}, \qquad \text{(A.23)}
\end{aligned}$$

where we have used (A.16) in the last equality. Following similar steps as in (A.22), and using (A.18) we get

$$\boldsymbol{\varepsilon}^* \left[\mathbf{P}\mathbf{A}_r\mathbf{A}^\dagger\right]_r \boldsymbol{\varepsilon} = -\mathbf{c}^*\mathbf{A}_r^*\mathbf{P}\mathbf{A}_r\mathbf{c}. \tag{A.24}$$

Hence using (A.18) and (A.24) we have

$$\begin{aligned} \boldsymbol{\varepsilon}^*\mathbf{P}_{rr}\boldsymbol{\varepsilon} &= -\boldsymbol{\varepsilon}^* \left[\mathbf{P}\mathbf{A}_r\mathbf{A}^\dagger\right]_r \boldsymbol{\varepsilon} - \left\{\boldsymbol{\varepsilon}^* \left[\mathbf{P}\mathbf{A}_r\mathbf{A}^\dagger\right]_r \boldsymbol{\varepsilon}\right\}^* \\ &= 2\mathbf{c}^*\mathbf{A}_r^*\mathbf{P}\mathbf{A}_i\mathbf{c}. \end{aligned} \tag{A.25}$$

To show (A.21) we proceed similarly as above to get

$$\begin{aligned} \boldsymbol{\varepsilon}^* \left[\mathbf{P}\mathbf{A}_r\mathbf{A}^\dagger\right]_i &= \mathbf{c}^*\mathbf{A}^* \left[\mathbf{P}_i\mathbf{A}_r\mathbf{A}^\dagger + \mathbf{P}\mathbf{A}_{ri}\mathbf{A}^\dagger + \mathbf{P}\mathbf{A}_i\left(\mathbf{A}^\dagger\right)_r\right]\mathbf{A}\mathbf{c} \\ &= \mathbf{c}^*\mathbf{A}^*\mathbf{P}_i\mathbf{A}_r\mathbf{A}^\dagger\mathbf{A}\mathbf{c} \\ &= -\mathbf{c}^*\mathbf{A}^* \left[\mathbf{P}\mathbf{A}_i\mathbf{A}^\dagger + \mathbf{A}\dagger*\mathbf{A}_i^*\mathbf{P}\right]\mathbf{A}_r\mathbf{c} \\ &= -\mathbf{c}^*\mathbf{A}^*\mathbf{A}^{\dagger*}\mathbf{A}_i^*\mathbf{P}\mathbf{A}_r\mathbf{c} \\ &= -\mathbf{c}^*\mathbf{A}_i^*\mathbf{P}\mathbf{A}_r\mathbf{c} = \mathrm{i}\mathbf{c}^*\mathbf{A}_r^*\mathbf{P}\mathbf{A}_r\mathbf{c}, \end{aligned} \tag{A.26}$$

which is a purely imaginary quantity. Note that we have used (A.12) in the last equality. Thus by (A.19) we have

$$\begin{aligned} \boldsymbol{\varepsilon}^*\mathbf{P}_{ri}\boldsymbol{\varepsilon} &= -\boldsymbol{\varepsilon}^* \left[\mathbf{P}\mathbf{A}_r\mathbf{A}^\dagger\right]_i \boldsymbol{\varepsilon} - \left\{\boldsymbol{\varepsilon}^* \left[\mathbf{P}\mathbf{A}_r\mathbf{A}^\dagger\right]_i \boldsymbol{\varepsilon}\right\}^* \\ &= 0. \end{aligned} \tag{A.27}$$

Hence the proposition is proved ■

We shall need the following results concerning the first order derivatives of the projection operator $\mathbf{P}(\mathbf{e}_\omega)$.

Proposition 4: The following results hold

$$\mathrm{tr}[\mathbf{P}_r(\mathbf{e}_\omega)] = \mathrm{tr}[\mathbf{P}_i(\mathbf{e}_\omega)] = 0, \tag{A.28}$$

$$\mathbf{P}_r(\mathbf{e}_\omega)\mathbf{P}_i(\mathbf{e}_\omega) + \mathbf{P}_i(\mathbf{e}_\omega)\mathbf{P}_r(\mathbf{e}_\omega) = 0, \tag{A.29}$$

$$\begin{aligned} \boldsymbol{\varepsilon}^*(\omega)\mathbf{P}_r^2(\mathbf{e}_\omega)\boldsymbol{\varepsilon}(\omega) &= \boldsymbol{\varepsilon}^*(\omega)\mathbf{P}_i^2(\mathbf{e}_\omega)\boldsymbol{\varepsilon}(\omega) \\ &= \mathbf{c}^*(\omega)\mathbf{A}_r^*(\mathbf{e}_\omega)\mathbf{P}(\mathbf{e}_\omega)\mathbf{A}_r(\mathbf{e}_\omega)\mathbf{c}(\omega) \end{aligned} \tag{A.30}$$

Proof: For the proof of (A.28) and (A.29), we refer the reader to [11]. While proving (A.30), we shall omit the argument $\mathbf{e}_\omega$ of matrices for convenience. From (A.18) and (3.10) we have

$$\begin{aligned} \boldsymbol{\varepsilon}^*\mathbf{P}_r^2\boldsymbol{\varepsilon} &= \boldsymbol{\varepsilon}^*\mathbf{P}_r\mathbf{P}_r\boldsymbol{\varepsilon} \\ &= \mathbf{c}^*\mathbf{A}^* \left[\mathbf{P}\mathbf{A}_r\mathbf{A}^\dagger\right]^* \left[\mathbf{P}\mathbf{A}_r\mathbf{A}^\dagger\right]\mathbf{A}\mathbf{c} \\ &= \mathbf{c}^*\mathbf{A}_r^*\mathbf{P}\mathbf{A}_r\mathbf{c}, \end{aligned} \tag{A.31}$$

where we have used $\mathbf{P}^*\mathbf{A} = 0$ in the second equality (which can be easily verified) and $\mathbf{P}^*\mathbf{P} = \mathbf{P}$ in the last equality. Similarly from (A.19) we get

$$\boldsymbol{\varepsilon}^*\mathbf{P}_i^2\boldsymbol{\varepsilon} = \mathbf{c}^*\mathbf{A}_i^*\mathbf{P}\mathbf{A}_i\mathbf{c} = \mathbf{c}^*\mathbf{A}_r^*\mathbf{P}\mathbf{A}_r\mathbf{c} \tag{A.32}$$

using (A.23). Hence the proposition is proved. ■

Proof of the theorem: Under the assumption of of high SNR, the estimate $\hat{\mathbf{e}}_\omega$ can be assumed to be close to the true parameter vector $\mathbf{e}_{\omega 0}$ and we can reasonably approximate the cost function $W(\mathbf{e}_\omega)$ by the truncated Taylor's series expansion in the neighbourhood of $\mathbf{e}_{\omega 0}$ as

$$W(\mathbf{e}_\omega) \approx W(\mathbf{e}_{\omega 0}) + W'(\mathbf{e}_{\omega 0})[\mathbf{e}_\omega - \mathbf{e}_{\omega 0}] + \frac{1}{2}[\mathbf{e}_\omega - \mathbf{e}_{\omega 0}]^{\mathrm{T}} W''(\mathbf{e}_{\omega 0})[\mathbf{e}_\omega - \mathbf{e}_{\omega 0}] \quad \text{(A.33)}$$

where we have neglected all higher terms. Differentiating (A.34) with respect to $\mathbf{e}_\omega$ and noting that $W'(\hat{\mathbf{e}}_\omega) = 0$, we have

$$\hat{\mathbf{e}}_\omega - \mathbf{e}_{\omega 0} \approx -\left[W''(\mathbf{e}_{\omega 0})\right]^{-1} W'(\mathbf{e}_{\omega 0}) \quad \text{(A.34)}$$

Thus for large SNR we can write using (A.35) that

$$C_{jk} \equiv E\left\{\left(\hat{\mathbf{e}}_{\omega_j} - \mathbf{e}_{\omega_j 0}\right)\left(\hat{\mathbf{e}}_{\omega_k} - \mathbf{e}_{\omega_k 0}\right)^{\mathrm{T}}\right\} \approx \mathbf{H}^{-1}(\omega_j)\mathbf{G}(\omega_j, \omega_k)\mathbf{H}^{-1}(\omega_k) \quad \text{(A.35)}$$

where we have introduced

$$\mathbf{G}(\omega_j, \omega_k) = E\left[W'(\mathbf{e}_{\omega_j 0}\right]\left[W'(\mathbf{e}_{\omega_k 0}\right]^*, \quad \text{(A.36)}$$

$$\mathbf{H}(\omega) = \lim_{\mathrm{SNR}\to\infty} W''\left(\mathbf{e}_{\omega 0}\right). \quad \text{(A.37)}$$

Note thet $\mathbf{H}(\omega)$ is a symmetric matrix. Since $\lim_{\mathrm{SNR}\to\infty} \mathbf{z}(\omega) = \boldsymbol{\varepsilon}(\omega)$, using (A.38) and (3.17) we get

$$\mathbf{H}(\omega) = \begin{bmatrix} \boldsymbol{\varepsilon}^*(\omega)\mathbf{P}_{rr}(\mathbf{e}_{\omega 0})\boldsymbol{\varepsilon}(\omega) & \boldsymbol{\varepsilon}^*(\omega)\mathbf{P}_{rr}(\mathbf{e}_{\omega 0})\boldsymbol{\varepsilon}(\omega) \\ \boldsymbol{\varepsilon}^*(\omega)\mathbf{P}_{rr}(\mathbf{e}_{\omega 0})\boldsymbol{\varepsilon}(\omega) & \boldsymbol{\varepsilon}^*(\omega)\mathbf{P}_{rr}(\mathbf{e}_{\omega 0})\boldsymbol{\varepsilon}(\omega) \end{bmatrix} = h(\omega)\mathbf{I}_2, \quad \text{(A.38)}$$

where we have used (3.21), (A.20) and (A.21) in the last eqality. Now let us consider the gradient of the cost function evaluated at the true parameter vector.

$$W'(\mathbf{e}_{\omega 0}) = \begin{bmatrix} \mathbf{z}^*(\omega)\mathbf{P}_r(\mathbf{e}_{\omega 0})\mathbf{z}(\omega) \\ \mathbf{z}^*(\omega)\mathbf{P}_i(\mathbf{e}_{\omega 0})\mathbf{z}(\omega) \end{bmatrix} = \begin{bmatrix} [\boldsymbol{\varepsilon}(\omega) + \mathbf{v}(\omega)]^* \mathbf{P}_r(\mathbf{e}_{\omega 0}) [\boldsymbol{\varepsilon}(\omega) + \mathbf{v}(\omega)] \\ [\boldsymbol{\varepsilon}(\omega) + \mathbf{v}(\omega)]^* \mathbf{P}_i(\mathbf{e}_{\omega 0}) [\boldsymbol{\varepsilon}(\omega) + \mathbf{v}(\omega)] \end{bmatrix}. \quad \text{(A.39)}$$

Note that,

$$\begin{aligned} \lim_{\mathrm{SNR}\to\infty} W'(\mathbf{e}_{\omega 0}) &= \begin{bmatrix} \boldsymbol{\varepsilon}^*(\omega)\mathbf{P}_r(\mathbf{e}_{\omega 0})\boldsymbol{\varepsilon}(\omega) \\ \boldsymbol{\varepsilon}^*(\omega)\mathbf{P}_i(\mathbf{e}_{\omega 0})\boldsymbol{\varepsilon}(\omega) \end{bmatrix} = \begin{bmatrix} \mathbf{c}^*(\omega)\mathbf{A}^*(\mathbf{e}_{\omega 0})\mathbf{P}_r(\mathbf{e}_{\omega 0})\mathbf{A}(\mathbf{e}_{\omega 0})\mathbf{c}(\omega) \\ \mathbf{c}^*(\omega)\mathbf{A}^*(\mathbf{e}_{\omega 0})\mathbf{P}_r(\mathbf{e}_{\omega 0})\mathbf{A}(\mathbf{e}_{\omega 0})\mathbf{c}(\omega) \end{bmatrix} \\ &= 0, \end{aligned} \quad \text{(A.40)}$$

where we have used

$$\mathbf{A}^*(\mathbf{e}_{\omega 0})\mathbf{P}_r(\mathbf{e}_{\omega 0})\mathbf{A}(\mathbf{e}_{\omega 0}) = \mathbf{A}^*(\mathbf{e}_{\omega 0})\mathbf{P}_i(\mathbf{e}_{\omega 0})\mathbf{A}(\mathbf{e}_{\omega 0}) = 0, \quad \text{(A.41)}$$

which follows from (A.18) and (A.19) using $\mathbf{P}(\mathbf{e}_\omega)\mathbf{A}(\mathbf{e}_\omega) = 0$. The equation (A.40) indicates the fact that the graduent of the cost function should vanish at the true parameter values as the SNR approaches infinity. For finite SNR using (A.1) and (A.40) we have

$$\begin{aligned} EW'(\mathbf{e}_{\omega 0}) &= E\begin{bmatrix} \mathbf{v}^*(\omega)\mathbf{P}_r(\mathbf{e}_{\omega 0})\mathbf{v}(\omega) \\ \mathbf{v}^*(\omega)\mathbf{P}_i(\mathbf{e}_{\omega 0})\mathbf{v}(\omega) \end{bmatrix} = \begin{bmatrix} \mathrm{tr}\left[\mathbf{P}_r(\mathbf{e}_{\omega 0})E\mathbf{v}(\omega)\mathbf{v}^*(\omega)\right] \\ \mathrm{tr}\left[\mathbf{P}_i(\mathbf{e}_{\omega 0})E\mathbf{v}(\omega)\mathbf{v}^*(\omega)\right] \end{bmatrix} \\ &= \sigma\begin{bmatrix} \mathrm{tr}\left[\mathbf{P}_r(\mathbf{e}_{\omega 0})\right] \\ \mathrm{tr}\left[\mathbf{P}_r(\mathbf{e}_{\omega 0})\right] \end{bmatrix} = 0. \end{aligned} \quad \text{(A.42)}$$

Here we have used (A.3) and (A.28). Since uncorrelated Gaussian random vectors are independent, we get by (A.36) and (A.42) for $j \neq k$

$$\mathbf{G}(\omega_j, \omega_k) = E\left[W'(\mathbf{e}_{\omega_j 0})\right] E\left[W'(\mathbf{e}_{\omega_k 0})\right]^* = 0. \tag{A.43}$$

Now for the same frequency, we shall use (A.36), (A.39 and (A.40) and apply (A.7). Neglecting the second order term in σ we have

$$\mathbf{G}(\omega_k, \omega_k) = \sigma \begin{bmatrix} 2\boldsymbol{\varepsilon}^* \mathbf{P}_r^2 \boldsymbol{\varepsilon} & \boldsymbol{\varepsilon}^* [\mathbf{P}_r \mathbf{P}_i + \mathbf{P}_i \mathbf{P}_r] \boldsymbol{\varepsilon} \\ \boldsymbol{\varepsilon}^* [\mathbf{P}_r \mathbf{P}_i + \mathbf{P}_i \mathbf{P}_r] \boldsymbol{\varepsilon} & 2\boldsymbol{\varepsilon}^* \mathbf{P}_i^2 \boldsymbol{\varepsilon} \end{bmatrix}, \tag{A.44}$$

where we have omitted the arguments of the matrices for convenience. Combining (A.29), (A.30) and (A.44) and using the definition (3.22) we get

$$\mathbf{G}(\omega_k, \omega_k) = \sigma h(\omega_k) \mathbf{I}_2. \tag{A.45}$$

Hence using (A.35), (A.38), (A.43) and (A.45) we get

$$C_{jk} = \frac{\sigma}{h(\omega)} \delta_{j,k} \mathbf{I}_2, \tag{A.46}$$

which completes the proof of the theorem. ■

B Proof of the lemma

We shall omit the arguments of the matrices for convenience. We stress that the proof given in this section is valid for any 4×4 full rank matrix $\mathbf{D}$ in (4.2). Though we have a specific structure of $\mathbf{D}$ in (4.1), that is not necessary in what follows here. Consider first the pseudoinverse $\mathbf{A_s}^\dagger$ of $\mathbf{A_s}$. We have from (4.2)

$$\mathbf{A_s}^\dagger = \left(\mathbf{A_s}^* \mathbf{A_s}\right)^{-1} \mathbf{A_s} = \left(\mathbf{D}^* \mathbf{A}^* \mathbf{A} \mathbf{D}\right)^{-1} \mathbf{D}^* \mathbf{A}^* = \mathbf{D}^{-1} \mathbf{A}^\dagger. \tag{B.1}$$

Here we have used the fact that $\mathbf{D}$ is full rank matrix. Consider the projection matrix $\mathbf{P_s}$. Using the definition,

$$\mathbf{P_s} = \mathbf{I}_n - \mathbf{A_s} \mathbf{A_s}^\dagger = \mathbf{I}_n - \mathbf{A} \mathbf{D} \mathbf{D}^{-1} \mathbf{A}^\dagger = \mathbf{P}. \tag{B.2}$$

Note that we used (B.1) in the last equality. From (B.2) and (4.3) follows directly. Next we shall prove (4.4). Using the definition (3.21) we get

$$\begin{aligned} h &= 2\boldsymbol{\varepsilon}^* \mathbf{A}^{\dagger *} \mathbf{A}_r \mathbf{P} \mathbf{A}_r \mathbf{A}^\dagger \boldsymbol{\varepsilon} \\ &= 2\boldsymbol{\varepsilon}^* \mathbf{A}^{\dagger *} \mathbf{D}^{-*} \mathbf{D}^* \mathbf{A}_r \mathbf{P} \mathbf{A}_r \mathbf{D} \mathbf{D}^{-1} \mathbf{A}^\dagger \boldsymbol{\varepsilon} \\ &= 2\boldsymbol{\varepsilon}^* \mathbf{A_s}^{\dagger *} \mathbf{D}^* \mathbf{A}_r \mathbf{P_s} \mathbf{A}_r \mathbf{D} \mathbf{A_s}^\dagger \boldsymbol{\varepsilon}, \end{aligned} \tag{B.3}$$

where we have used (B.1) and (B.2) in the last equality. With this observation, we have proved the lemma. ■

C Computation of $\mathbf{A}_r(\mathbf{e}_\omega)$

From (4.4) we note $\mathbf{A}_r(\mathbf{e}_\omega)$ is required to compute the expected variance of the parameter estimates. In this section we show explicitely the calculations involved in the computation of $\mathbf{A}_r(\mathbf{e}_\omega)$. We shall stick to the notations (A.11)-(A.15). For convenience we drop the frequency arguments of the variables. Differentiating (2.6) and (2.7) with respect to $e_r(\omega)$ we have

$$a_r = -\frac{\rho\omega^2}{2\mathcal{E}(\omega)^2}[1+\psi], \tag{C.1}$$

$$b_r = -\frac{\rho\omega^2 A}{\mathcal{E}(\omega)^2 I} + \frac{2\rho^2\omega^4\psi}{\mathcal{E}(\omega)^3}. \tag{C.2}$$

Differentiating (2.8) we get

$$\begin{aligned} 2aa_r + b_r &= 2\left(\gamma_1^2 + a\right)(2\gamma_1\gamma_{1r} + a_r) \\ \Rightarrow \gamma_{1r} &= \frac{1}{2\gamma_1}\left[\frac{2aa_r + b_r}{2\left(\gamma_1^2 + a\right)} - a_r\right]. \end{aligned} \tag{C.3}$$

Similarly differentiation (2.9) we get

$$\gamma_{2r} = \frac{1}{2\gamma_2}\left[\frac{2aa_r + b_r}{2\left(\gamma_2^2 + a\right)} - a_r\right]. \tag{C.4}$$

Let us introduce the diagonal matrices

$$\mathbf{X} = \begin{bmatrix} x_1 & & \\ & \ddots & \\ & & x_n \end{bmatrix}, \tag{C.5}$$

$$\mathbf{\Gamma}_r = \begin{bmatrix} \gamma_{1r} & & & \\ & \gamma_{2r} & & \\ & & -\gamma_{1r} & \\ & & & -\gamma_{2r} \end{bmatrix}. \tag{C.6}$$

Then by differentiating (3.11) with respect to $e_r(\omega)$ we get

$$\mathbf{A}_r = \mathbf{X}\mathbf{A}\mathbf{\Gamma}_r. \tag{C.7}$$

References

[1] R. H. Blanc. Transient wave propagation methods for determining the viscoelastic properties of solids. *Journal of Applied Mechanics*, 60:763–768, 1993.

[2] C. Casula and J. M. Caricoine. Generalized mechanical model analogies of linear viscoelastic behaviour. *Bollettino di Geofisica Teorica ed Applicata*, 34:235–256, 1992.

[3] R. V. Churchill and J. W. Brown. *Complex Variables and Applications*. McGraw-Hill, 4th edition, 1989.

[4] W. Flügge. *Viscoelasticity.* Springer-Verlag, 2nd edition, 1975.

[5] G. H. Golub and C. F. Van Loan. *Matrix Computations, 2nd ed.* John Hopkins University Press, Baltimore, MD, USA, 1989.

[6] G. H. Golub and V. Pereyra. The differentiation of pseudo-inverses and nonlinear least squares problems whose variables separate. *SIAM journal of Numerical Analysis*, 10(2):413–432, 1973.

[7] L. Hillström and B. Lundberg. Analysis of elastic flexural waves in non-uniform beams based on measurement of strains and accelarations. *Journal of Sound and Vibration*, 246:227–242, 2001.

[8] L. Hillström, M. Mossberg, and B. Lundberg. Identification of complex modulus from measured strains on an axially impacted bar using least squares. *Journal of Sound and Vibration*, 230:689–707, 2000.

[9] P. Janssen and P. Stoica. On the expectation of the product of four matrix-valued gaussian random variables. *IEEE Trans. Automatic Control*, AC-33:867–870, 1988.

[10] B. Lundberg and R. H. Blanc. Determination of mechanical material properties from the two-point response of an impacted linearly viscoelastic rod specimen. *Journal of Sound and Vibration*, 126(1):97–108, 1988.

[11] M. Mossberg, L. Hillström, and T. Söderström. Non-parametric identification of viscoelastic materials from wave propagation experiments. *Automatica*, 37(4):511–521, April 2001.

[12] A. V. Oppenheim and R. W. Schafer. *Discrete-Time Signal Processing.* Prentice Hall International, Englewood Cliffs, New Jersey, 1975.

[13] T. Söderström and P. Stoica. *System Identification.* Prentice Hall International, Hemel Hempstead, UK, 1989.

[14] G. W. Stewart. On the perturbation of pseudo-inverses, projections and linear least squares problem. *SIAM Review*, 19:634–662, 1977.